ATLAS studies on Higgs to diboson states

F. HUBAUT,
On behalf of the ATLAS Collaboration.
CPPM, Aix-Marseille Université, CNRS/IN2P3,
163 Av. de Luminy, Case 902, 13288 Marseille Cedex 9, France

The latest studies on the observed Higgs-like boson performed by the ATLAS experiment in diboson channels are reported. Emphasis is given to the property measurements (mass, spin-parity, couplings) of the new boson, that are driven by these channels. Most of them exploit the whole data sample of 20.7 fb^{-1} collected at the LHC in 2012 at $\sqrt{s} = 8$ TeV and 4.8 fb^{-1} collected in 2011 at $\sqrt{s} = 7$ TeV.

1 Introduction

Diboson states were at the core of the Higgs-like boson discovery published last Summer by the ATLAS and CMS collaborations [1,2], based on $\gamma\gamma$, $ZZ^{(*)} \to 4l$ and $WW^{(*)} \to l\nu l\nu$ final states. Since then, ATLAS Higgs to diboson states analyses mostly focused on refining the property measurements (mass, spin-parity, couplings) of the new boson, that are driven by these channels. In the following, updated $H \to \gamma\gamma$ and $H \to ZZ^{(*)} \to 4l$ analyses are reported, exploiting the whole LHC proton-proton collision dataset of 20.7 fb^{-1} at $\sqrt{s} = 8$ TeV and 4.8 fb^{-1} at $\sqrt{s} = 7$ TeV recorded by the ATLAS detector [3]. Besides the benefit from an increased data sample, they have been further improved to be more sensitive to the vector-boson fusion ($qq' \to qq'H$, denoted VBF) and Higgs-strahlung ($qq' \to WH/ZH$, denoted VH) production modes, largely sub-dominant ($\sim 10\%$) with respect to the gluon fusion process ($gg \to H$, denoted ggF) in the Standard Model (SM). These updated results are complemented with an analysis in the $H \to WW^{(*)} \to l\nu l\nu$ channel and a first search in the $H \to Z\gamma$ decay channel. Diboson states are also at the core of dedicated Higgs boson searches at high mass ($150 - 1000$ GeV), that need to be re-interpreted in light of the new boson discovery. In this respect, an updated $H \to ZZ \to 4l$ analysis, using the whole data sample and searching for other possible signals of beyond Standard Model Higgs(es) at high mass, is reported.

2 Updated results in the $H \to \gamma\gamma$ channel and property measurements

The $H \to \gamma\gamma$ decay channel provides a clean final-state topology with two isolated photons with high transverse energy, allowing the resonance mass to be reconstructed with high precision. The analysis [4] exploits the whole data sample of 20.7 fb^{-1} collected in 2012 at $\sqrt{s} = 8$ TeV and 4.8 fb^{-1} collected in 2011 at $\sqrt{s} = 7$ TeV. It searches for a localized excess of diphoton events over a smoothly falling background due to prompt diphoton production and to events with at least one jet misidentified as a photon. The two main experimental handles are therefore background reduction and invariant mass resolution. For the former, pile-up robust photon identification criteria are associated with track- and calorimeter-based isolation requirements, resulting in a $\sim$40% signal event efficiency. This allows to reduce the γ-jet and jet-jet backgrounds well below ($\sim$25%) the irreducible $\gamma\gamma$-continuum ($\sim$75%), as measured with data-driven techniques over the explored mass range from 100 GeV to 160 GeV. The angular term in the diphoton mass resolution is negligible thanks to the use of the calorimeter longitudinal segmentation to compute the so-called 'photon pointing', that is further fed in a multivariate discriminant exploiting also tracking information. This allows to reconstruct the diphoton primary vertex location with high efficiency even in high pile-up conditions. The overall inclusive diphoton mass resolution, dominated by the energy resolution, is 1.77 GeV, shown to be very stable with time and pile-up conditions. The signal-to-background ratio in a mass window around $m_H = 125$ GeV containing 90% of the expected signal is 3%. The inclusive invariant mass distribution of the 142 681 diphoton candidates reconstructed in the range $100 < m_{\gamma\gamma}$ [GeV]< 160 is shown in Figure 1 (left) with overlaid signal-plus-background fit.

To increase the sensitivity of the signal measurement, the selected events in the 8 TeV data sample are divided into 14 exclusive categories based on event properties (the 7 TeV analysis is unchanged with respect to Ref. [5]). The categorisation has been re-optimised to favour coupling measurements, five categories being designed to increase the sensitivity to the VBF and VH production processes. They are based on the selection of different objects, like one lepton or high missing transverse energy or two jets with small rapidity separation for the VH mode. None of the categories targeting a particular production mode are 100% pure and all have an admixture of other production mechanisms. Compared to the previous analysis [5], new categories enriched in associated production with vector bosons have been introduced and a multivariate analysis - exploiting the full event topology and the correlation between photon and jet kinematic quantities - is performed to improve the sensitivity to the VBF production mode. As an example, the expected purity in VBF events is improved to 75% in the best dedicated category, where 8.1 signal events are expected. The nine other categories differ in signal-to-background ratio (from 1% to 16%) as well as invariant mass resolution (from 1.4 to 2.5 GeV). In each category, the signal is extracted by a signal-plus-background fit to the invariant mass distribution.

The excess of events around $m_H = 126.5$ GeV seen in Figure 1 (left) is quantified in Figure 1 (right), showing the local p_0 value, *i.e.* the probability of the background fluctuating beyond the observation in the combined 7 TeV and 8 TeV dataset. The largest local significance is observed to be 7.4 σ at $m_H = 126.5$ GeV, while the expected significance is 4.1 σ. The largest observed (expected) local significance for the inclusive analysis is 6.1 (2.9) σ. The best-fit values of the signal strength μ, defined as a scale factor of the number of signal events expected from the SM Higgs boson hypothesis, and m_H are shown in Figure 2 (left). The measured value of the mass is $126.8 \pm 0.2(\text{stat}) \pm 0.7(\text{syst})$ GeV, where the systematic error is largely dominated by the uncertainties on the photon energy scale. At this best-fit mass, the signal strength μ is measured to be $1.65^{+0.34}_{-0.30}$, consistent across the various categories within their uncertainties. The total uncertainty is fairly shared between the statistical component (± 0.24) and the systematic

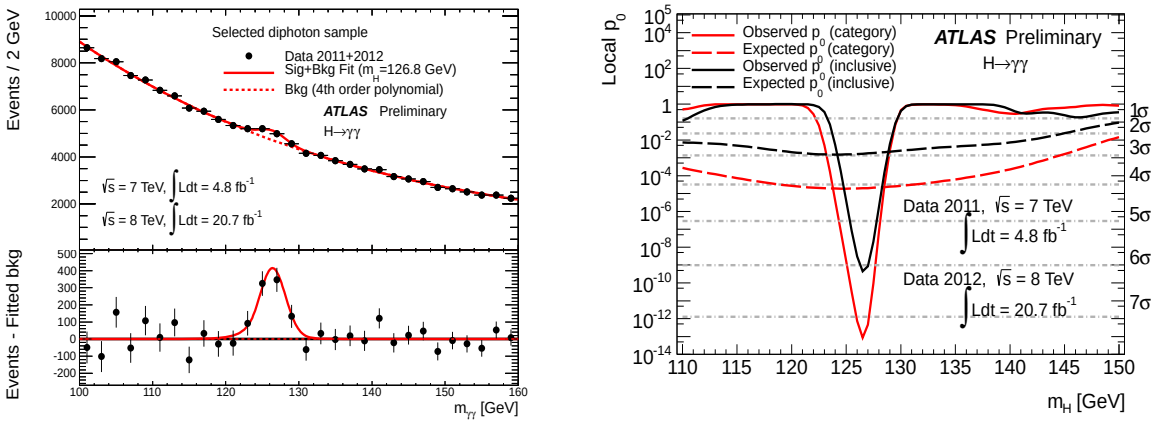

Figure 1: Left: Invariant mass distribution of the selected diphoton candidates in the combined $\sqrt{s} = 7$ TeV and $\sqrt{s} = 8$ TeV data samples. The result of a fit including a signal component fixed to m_H=126.8 GeV and a background one described by a fourth order Bernstein polynomial is superimposed. The bottom inset displays the data residuals with respect to the fitted background. Right: Observed (full line) and expected (dashed line) local p_0-value as a function of m_H, for the categorised analysis (red) and the fully inclusive analysis (black). Ref.[4].

one $(^{+0.25}_{-0.18})$, which includes experimental uncertainties on the signal yield, signal resolution and migration between categories and theoretical uncertainties on the inclusive Higgs boson production cross section and decay branching ratio. The compatibility in the signal strength parameter between the data and the SM Higgs boson signal plus background hypothesis is estimated to be at the 2.3 σ level.

The event categories targeting different Higgs production modes allow to perform measurements on the signal strength of these individual modes. In Figure 2 (right), the ggF and ttH processes (resp. the VBF and VH processes), involving the coupling between a Higgs boson and top quarks (resp. gauge bosons), are grouped together to share the same signal strength parameter $\mu_{ggF+ttH}$ (resp. μ_{VBF+VH}). The fitted signal strengths are multiplied by a common scale factor B/B_{SM}, where B is the branching ratio for $H \to \gamma\gamma$ and B_{SM} is the branching ratio predicted by the SM. The best fit to the full dataset is in agreement with the SM expectations at the 2 σ level. The measurement has also been performed separating the VBF and VH production modes and the best-fit values for the signal strengths, displayed in Figure 3 (left), are:

$$\begin{aligned}
\mu_{\mathrm{ggF+ttH}} \times B/B_{\mathrm{SM}} &= 1.6^{+0.3}_{-0.3}(\mathrm{stat})^{+0.3}_{-0.2}(\mathrm{syst}) \\
\mu_{\mathrm{VBF}} \times B/B_{\mathrm{SM}} &= 1.7^{+0.8}_{-0.8}(\mathrm{stat})^{+0.5}_{-0.4}(\mathrm{syst}) \\
\mu_{\mathrm{VH}} \times B/B_{\mathrm{SM}} &= 1.8^{+1.5}_{-1.3}(\mathrm{stat})^{+0.3}_{-0.3}(\mathrm{syst})
\end{aligned} \quad (1)$$

Compared to the last public results[5], the related uncertainties have been improved by ∼30% (∼45%) for the VBF (VH) production signal strengths, thanks to the use of the full 2011+2012 statistics and to the re-optimised categorisation. The sensitivity to the VBF production mode is further quantified in Figure 3 (right), showing the local p_0^{VBF} value as a function of m_H for a SM Higgs boson signal produced in VBF. The other Higgs production modes are considered as background and their respective signal strengths are treated as nuisance parameters. The observed (expected) significance at the best-fit mass $m_H = 126.8$ GeV is 2.0 σ (1.3 σ).

A first measurement of the fiducial cross section for the production of the observed particle times branching ratio to the two photon decay mode has been performed, using 20.7 fb^{-1} of data at $\sqrt{s} = 8$ TeV. The fiducial region is defined, for isolated photons, by the kinematic range $E_T^{\gamma 1} > 40$ GeV, $E_T^{\gamma 2} > 30$ GeV and $|\eta^\gamma| < 2.37$. The measurement, 56.2 ±

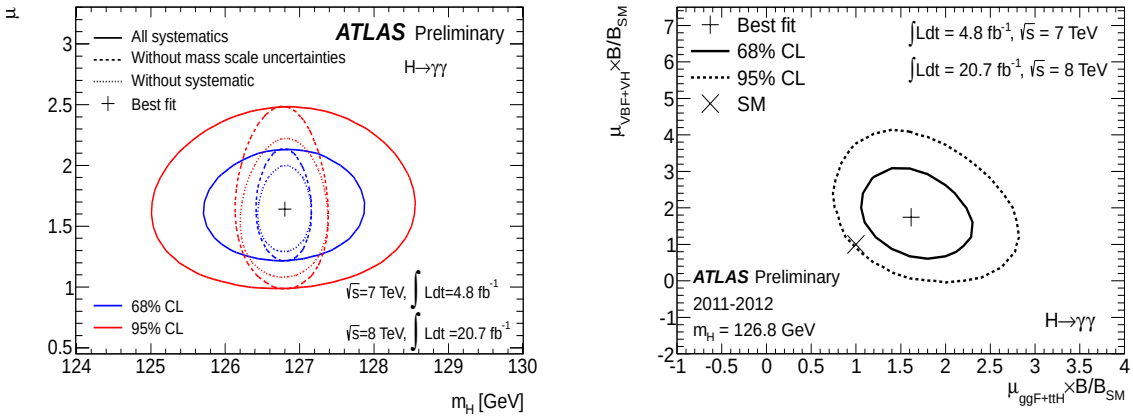

Figure 2: Left: Best-fit values (+) of m_H and μ, and their 68% (blue) and 95% (red) confidence level (CL) contours. Right: Best-fit values (+) of $\mu_{ggF+ttH} \times B/B_{SM}$ and $\mu_{VBF+VH} \times B/B_{SM}$ and their 68% (solid) and 95% (dashed) CL contours. The expectation for a SM Higgs boson is also shown (×). Ref.[4].

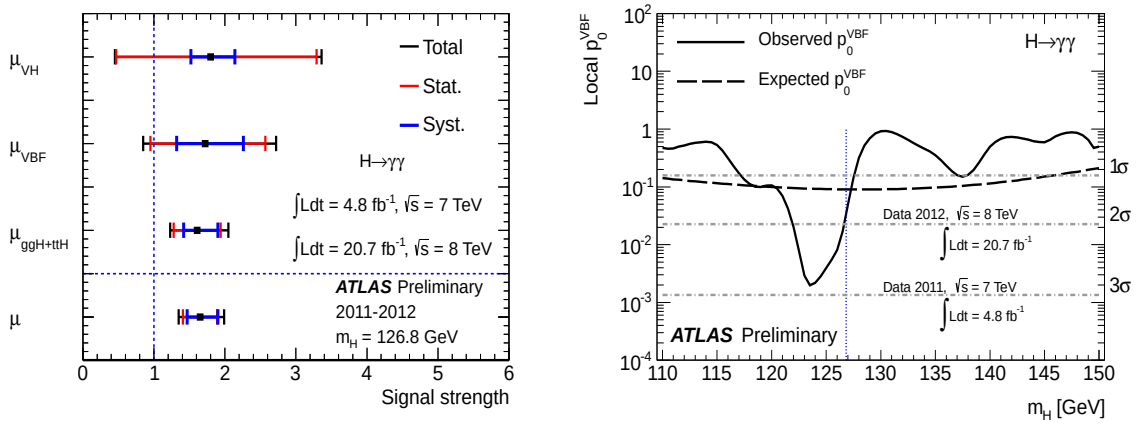

Figure 3: Left: Measured signal strengths $\mu_{ggF+ttH}$, μ_{VBF} and μ_{VH} for the different Higgs production modes. Right: Observed (solid black line) and expected (dashed curve) local p_0^{VBF} value for VBF $H \to \gamma\gamma$ production as a function of m_H. The vertical dotted line indicates the best-fit mass $m_H = 126.8$ GeV. Ref.[4].

10.5(stat)±6.5(syst)±2.0(lumi) fb, is compatible with the SM Higgs signal prediction measured using the same sample.

The spin property of the new particle is studied in the $\gamma\gamma$ decay channel by comparing the distribution of the photon polar angle θ^* in the resonance rest frame measured in the data to those predicted by the SM and by specific spin-2 models (graviton-like spin-2 state with minimal couplings). The analysis presented here [5] uses 13 fb^{-1} of 8 TeV data [a]. It is performed without categorisation in the signal region defined by the diphoton invariant mass range [123.8,128.6] GeV around the resonance peak. The background $|\cos\theta^*|$ distribution is determined from data, using the events in the sidebands of the diphoton invariant mass distribution. The main systematic uncertainty arises from the statistical component of the extrapolation procedure from the sidebands to the signal region. The observation is fully compatible with the SM 0^+ hypothesis, which is slightly favoured over the spin-2^+ hypothesis. The discrimination is largest for a spin-2 state produced via gluon fusion (with a 87% exclusion confidence level using CL_S), and decreases as expected with an increasing fraction of quark annihilation production process.

[a] It has been updated with the full statistics shortly after the conference, see Ref. [6].

3 Updated results in the $H \to ZZ^{(*)} \to 4$ leptons channel and property measurements

The $H \to ZZ^{(*)} \to 4l$ ($l = e, \mu$) decay channel provides a clean signature (two pairs of opposite-sign same-flavour isolated leptons) with a very low level of background and a fully reconstructed final state with excellent mass resolution. The analysis [7] exploits the whole data sample of 20.7 fb^{-1} collected in 2012 at $\sqrt{s} = 8$ TeV and 4.8 fb^{-1} collected in 2011 at $\sqrt{s} = 7$ TeV. Because of the small SM cross section times branching ratio (~2.5 fb at $\sqrt{s} = 8$ TeV for $m_H = 125$ GeV), high lepton acceptance, reconstruction and identification efficiencies are crucial down to low p_T (set to 6/7 GeV for muons/electrons in this analysis). The combined signal reconstruction and selection efficiency for a SM Higgs boson with $m_H = 125$ GeV in the 8 TeV data is ~40% for the 4μ channel and ~20% for the $4e$ channel. The impact on the reconstructed invariant mass of photon emission from final state radiation (FSR) is modelled by the simulations. All leading di-muon pair candidates with $66 < m_{\mu\mu}$ [GeV]< 89 are corrected for FSR by including in the invariant mass any selected photon with a reconstructed transverse energy above 1 GeV. This correction applies to ~4% of all $H \to ZZ^{(*)} \to 4\mu$ candidate events, in good agreement between data and Monte Carlo. The 4-lepton invariant mass resolution is improved by applying a Z-mass constrained kinematic fit to the leading lepton pair for $m_{4l} < 190$ GeV and to both lepton pairs for higher masses. The typical mass resolutions for $m_H = 125$ GeV are 1.3% and 1.9% for the 4μ and $4e$ sub-channels, respectively.

The largest background comes from continuum $(Z^{(*)}\gamma^*)(Z^{(*)}\gamma^*)$ production, referred to hereafter as $ZZ^{(*)}$, estimated using MC simulations normalised to the theoretical cross section. For low masses there are also important background contributions from Z+jets and $t\bar{t}$ production, where charged lepton candidates arise either from decays of hadrons with b- or c-quark content, from photon conversions or from jet mis-identification. Such reducible backgrounds are suppressed with impact parameter and track- and calorimeter-based isolation requirements. They are measured from various background-enriched control regions in data, whose yields are extrapolated to the signal region through transfer factors obtained from MC simulations and checked in data.

The invariant mass distribution of the selected four-lepton candidates reconstructed in the range $80 < m_{4l}$ [GeV]< 250 is shown in Figure 4 (left), together with the expectations for the backgrounds and the $m_H = 125$ GeV signal hypothesis. In the high-mass region $m_{4l} > 160$ GeV, 376 events are observed, in good agreement with the background expectations, 348 ± 26 events, largely dominated by $ZZ^{(*)}$. In the signal region $120 < m_{4l}$ [GeV]< 130, 11.1 ± 1.3 background events are expected while 15.9 ± 2.1 events are expected for a $m_H = 125$ GeV Higgs signal, leading to an overall signal-to-background ratio of 1.4. In this region, 32 events are observed. Their two-dimensional distributions of leading versus subleading dilepton invariant masses, displayed in Figure 4 (right), are in good agreement with the Monte Carlo expectations.

The excess of events around $m_H = 125$ GeV seen in Figure 4 (left) is quantified in Figure 5 (left), showing the local p_0 value as a function of the hypothesised Higgs mass. The largest local significance is observed to be 6.6 σ at $m_H = 124.3$ GeV - above the 5 σ mark for this individual channel as for the $\gamma\gamma$ case -, while the expected significance is 4.4 σ. The best-fit values of the signal strength μ and m_H are shown in Figure 5 (right). The measured value of the mass is $124.3^{+0.6}_{-0.5}(\text{stat})^{+0.5}_{-0.3}(\text{syst})$ GeV, the total error of ~0.5% being slightly dominated by the statistical component and the systematic error being dominated by the energy and momentum scale uncertainties. At this best-fit mass, the signal strength μ is measured to be $1.7^{+0.5}_{-0.4}$.

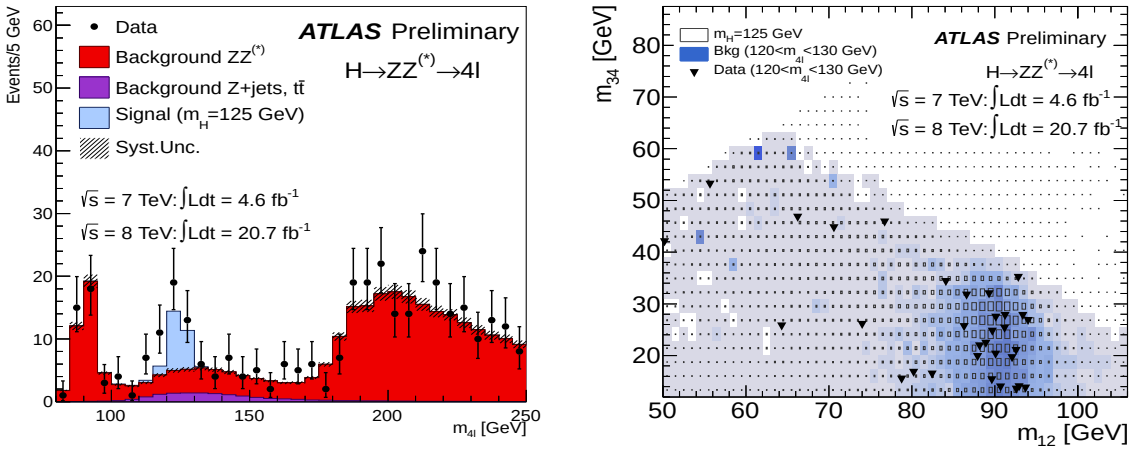

Figure 4: Left: Invariant mass distribution of the selected four-lepton candidates in the combined $\sqrt{s} = 7$ TeV and $\sqrt{s} = 8$ TeV data samples, compared to the background expectation in the 80-250 GeV mass range. The signal expectation for a SM Higgs with $m_H = 125$ GeV is also shown. Right: Distribution of the leading versus subleading dilepton invariant masses, before the application of the Z- mass constrained kinematic fit, for the 32 selected candidates in the m_{4l} range 120-130 GeV. The expected distributions for a SM Higgs with $m_H = 125$ GeV (the sizes of the boxes indicate the relative density) and for the total background (the intensity of the shading indicates the relative density) are also shown. Ref.[8].

The use of the whole data sample allows to further split the selected events in three different categories, designed to increase the sensitivity to the VBF and VH production processes. Events entering in the VBF-enriched category have two reconstructed jets with a large pseudo-rapidity separation ($|\Delta\eta_{jj}| > 3$) and a high dijet mass ($m_{jj} > 350$ GeV). In the high-mass region $m_{4l} > 160$ GeV, 6 events are observed in this category, in good agreement with the background expectations, 3.8 ± 1.3 events, largely dominated by $ZZ^{(*)}$. In the signal region $120 < m_{4l}$ [GeV]< 130, 0.71 ± 0.10 events are expected for a $m_H = 125$ GeV Higgs signal, with a 60% purity in VBF-produced events and a signal-to-background ratio around 5. In this region, 1 event is observed. This categorisation allows to perform measurements on the signal strength of the different Higgs production modes. In Figure 6 (left), the ggF and ttH processes (resp. the VBF and VH processes), involving the coupling between a Higgs boson and top quarks (resp. gauge bosons), are grouped together to share the same signal strength parameter $\mu_{ggF+ttH}$ (resp. μ_{VBF+VH}). The fitted signal strengths are muliplied by a common scale factor B/B_{SM}, where B is the branching ratio for $H \to ZZ^{(*)} \to 4l$ and B_{SM} is the branching ratio predicted by the SM. The measured values for $\mu_{\mathrm{ggF}+t\bar{t}H} \times B/B_{\mathrm{SM}}$ and $\mu_{\mathrm{VBF+VH}} \times B/B_{\mathrm{SM}}$ are $1.8^{+0.8}_{-0.5}$ and $1.2^{+3.8}_{-1.4}$, respectively. Further coupling interpretations of these results are presented elsewhere [8].

This channel provides a good sensitivity to search for an additional Higgs-like boson over a wide mass range. As no excess is observed in the data over the expected background in the mass range 200 GeV-1 TeV, upper limits are set on the production cross sections times branching ratio, assuming the signal to have a SM-like width, estimated using the complex-pole-scheme (CPS) [9]. The limits are derived separately for the ggF and the combined VBF/VH production mechanisms using the event categorisation described above, as illustrated in Figure 6 (right) for the gluon fusion production case.

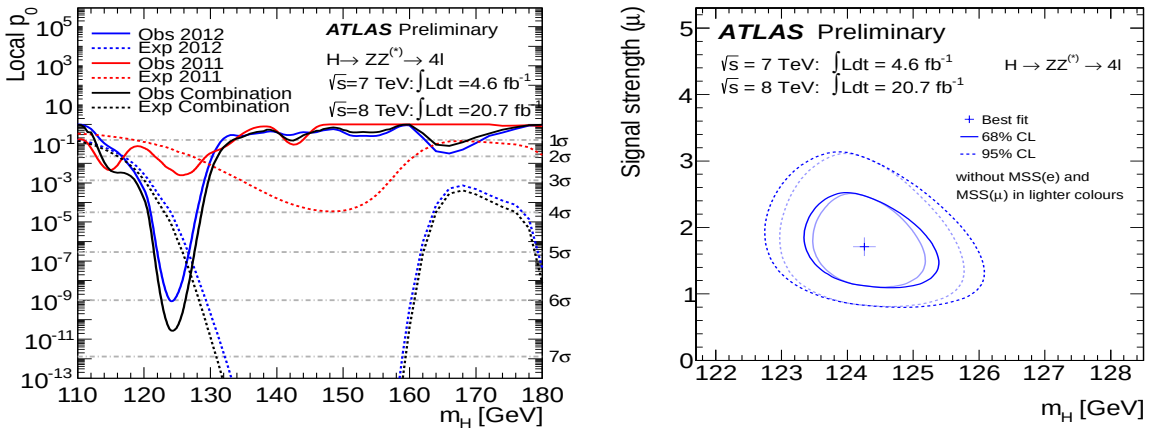

Figure 5: Left: Observed (full lines) and expected (dashed lines) local p_0-value as a function of m_H, for the 2011 dataset (red), the 2012 dataset (blue) and the combined dataset (black). Right: Best-fit values (+) of m_H and μ, and their 68% (blue) and 95% (red) confidence level (CL) contours. Ref.[8].

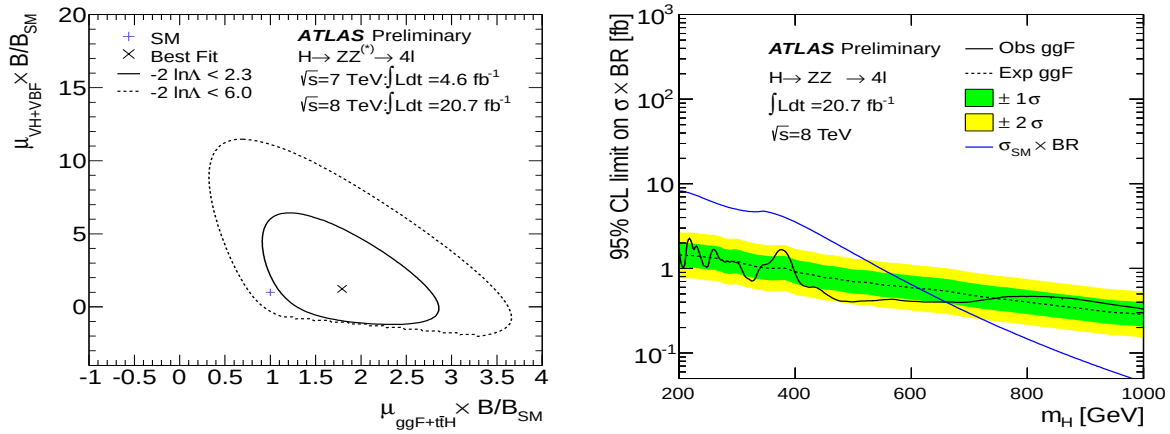

Figure 6: Left: Best-fit values (×) of $\mu_{ggF+ttH} \times B/B_{SM}$ and $\mu_{VBF+VH} \times B/B_{SM}$ and their 68% (solid) and 95% (dashed) CL contours. The expectation for a SM Higgs boson is also shown (+). Right: Observed (full black line) and expected (dashed line) 95% confidence limits on the production cross section times branching ratio of $H \to ZZ^{(*)} \to 4l$ ($l = e, \mu$) for a SM-like width signal produced through gluon-fusion, as a function of m_H. The green and yellow bands correspond to the $\pm 1\sigma$ and $\pm 2\sigma$ intervals. The expected SM cross section times branching ratio is also presented (blue line). Ref.[8].

A spin-parity analysis is performed on the 43 events with a reconstructed four-lepton invariant mass in the range $115 < m_{4l}$ [GeV]< 130. It exploits the kinematics of the production and decay of the events (one production angle, four decay angles and the two $Z^{(*)}$ boson masses) to build discriminants sensitive to the new boson spin-parity. Hypothesis tests comparing the SM 0^+ hypothesis with 0^-, 1^+, 1^-, 2^+ and 2^- have been performed, assuming a pure gluon fusion production. The scalar 0^+ hypothesis has also been compared to the 2^+ hypothesis for varying fractions of gluon fusion and quark annihilation production. The expected separation is found to be independent of the production fractions. The Higgs-like boson is found to be compatible with the SM expectation of 0^+ when compared pair-wise with 0^-, 1^+, 1^-, 2^+ and 2^-. The 0^- and 1^+ states are excluded at the 97.8% confidence level or higher using CL_S in favour of 0^+, as illustrated in Figure 7 for the pseudo-scalar 0^- case.

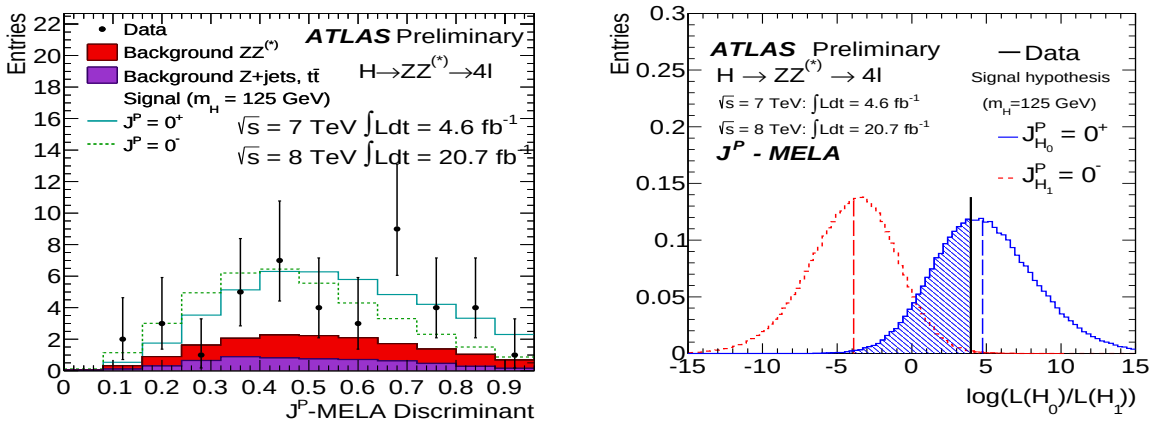

Figure 7: Left: Distribution of the spin-parity discriminant built for the 0^+ versus 0^- hypothesis test, for data and Monte Carlo expectations. Right: Distributions of the log-likelihood ratio generating with pseudo-experiments when assuming the spin-0^+ hypothesis and testing the 0^- hypothesis. The log-likelihood value observed in the data is indicated by the solid vertical line, and the medians of each of the expected distributions are indicated by dashed lines. Ref.[8].

4 Analysis in $H \to WW^{(*)} \to l\nu l\nu$ channel with 13 fb^{-1} of 8 TeV data

The signature for the $H \to WW^{(*)} \to l\nu l\nu$ channel is two high p_T opposite-charge leptons and a large missing transverse energy in the event due to the escaping neutrinos. This channel has a high rate, but limited mass resolution and a complex mixture of large backgrounds. The analysis presented here[10] uses 13 fb^{-1} of 8 TeV data[b], so only a short description is given. It uses final states with different-flavour leptons and 0 or 1 jet. The main backgrounds (WW, $t\bar{t}$, W+jets) are estimated from signal-free control regions in data. A broad excess of events is observed over the expected background, as seen in Figure 8 (left). It is quantified in Figure 8 (right), showing the local p_0 value as a function of the hypothesised Higgs mass. Due to the limited mass resolution in this channel, the p_0 distribution is rather flat around $m_H = 125$ GeV. The local observed (expected) significance of the excess is 2.6 σ (1.9 σ) at $m_H = 125$ GeV. At this mass value, the signal strength μ is measured to be 1.5 ± 0.6, where the total error is slightly dominated by the systematic uncertainty.

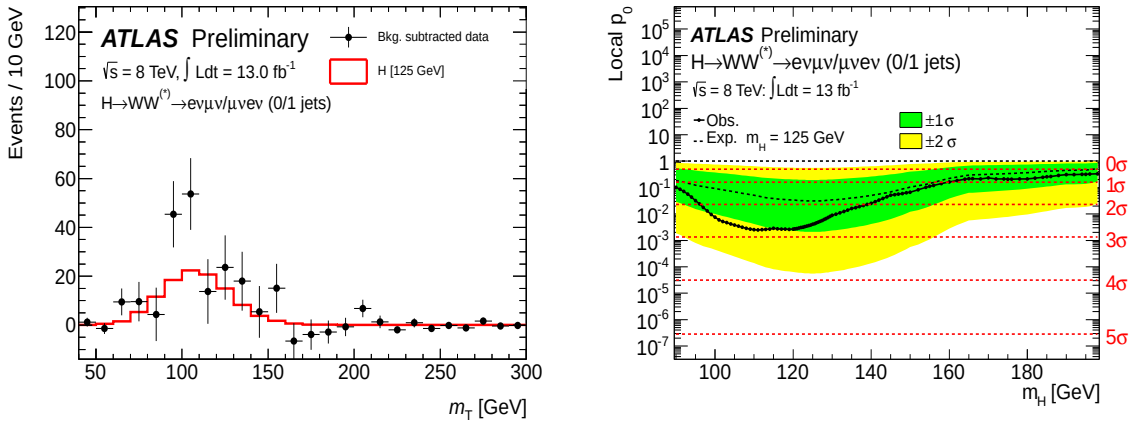

Figure 8: Left: Reconstructed transverse mass distribution in data, with the total estimated background subtracted. Only statistical uncertainties are displayed. The predicted signal for $m_H = 125$ GeV is overlaid. Right: Observed (full line) local p_0-value as a function of m_H. The dashed line indicates the corresponding expectation for the $m_H = 125$ GeV hypothesis, with its $\pm 1\sigma$ (green) and $\pm 2\sigma$ (yellow) uncertainty bands. Ref.[10].

[b] It has been updated with the full statistics shortly after the conference, see Ref. [11].

5 First search for the SM Higgs boson in the $H \to Z\gamma$ decay channel

The large integrated luminosity of the whole data sample (20.7 fb^{-1} at $\sqrt{s} = 8$ TeV and 4.6 fb^{-1} at $\sqrt{s} = 7$ TeV) is exploited to perform a first search in the rare decay channel $H \to Z\gamma$, $Z \to l^+l^-$ ($l = e, \mu$) [12]. This decay occurs through loop diagrams, making it particularly sensitive to the potential presence of new heavy particles and complementary to the $H \to \gamma\gamma$ decay channel. The SM cross section times branching ratio is ~2 fb at $\sqrt{s} = 8$ TeV for $m_H = 125$ GeV. With a ~30% event selection efficiency, 15 signal events are therefore expected to be selected in the whole data sample. The main SM backgrounds originate from $Z + \gamma$ events and production of Z+jets with one jet misidentified as a photon. The latter contribution is measured with data-driven techniques to be well below (~17%) the irreducible $Z+\gamma$ contribution (~82%). The total amount of background is directly fitted to the data mass spectrum, using the difference Δm between the final state three-body invariant mass $m_{ll\gamma}$ and the di-lepton invariant mass m_{ll} as discriminating variable. No significant deviation from the SM background prediction is observed, as illustrated in Figure 9 (left) in the muon channel for the $\sqrt{s} = 8$ TeV data sample. Upper limits on the cross section of a Higgs boson with a mass between 120 and 150 GeV are therefore derived, as shown in Figure 9 (right). For a Higgs boson mass of 125 GeV, the observed (resp. expected) limit is 18.2 (resp. 13.5) times the Standard Model. The results are dominated by the statistical uncertainties.

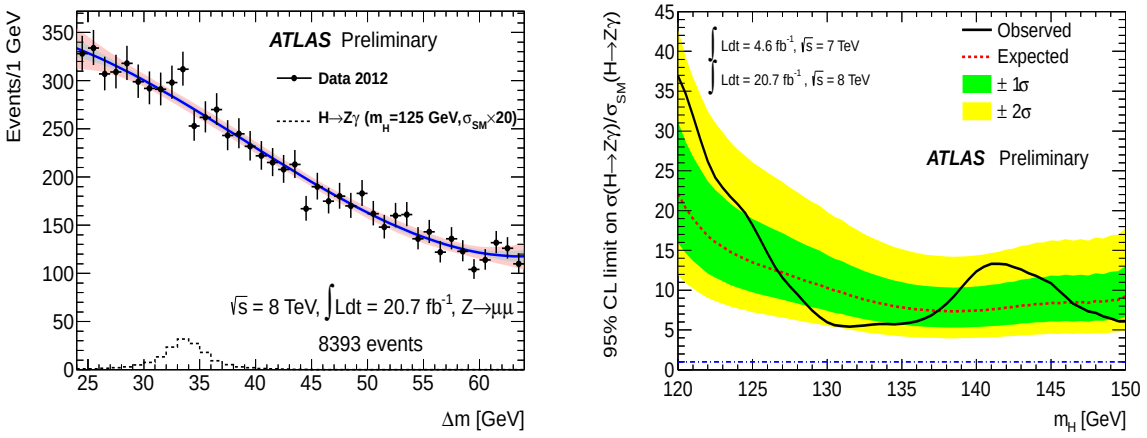

Figure 9: Left: $\Delta m = m_{\mu\mu\gamma} - m_{\mu\mu}$ distribution of the selected candidates in the $\sqrt{s} = 8$ TeV data sample. The result of a background-only fit with a third order Chebychev polynomial is superimposed. The dashed histogram corresponds to the SM signal expectation, for a Higgs boson mass of 125 GeV, scaled by a factor 20. Right: Observed (full line) and expected (dashed line) 95% confidence limits on the production cross section of a SM Higgs boson decaying to $Z\gamma$, as a function of the Higgs boson mass. The green and yellow bands correspond to the $\pm 1\sigma$ and $\pm 2\sigma$ intervals. Ref.[12].

6 Summary

First and preliminary analyses of the Higgs-like boson in $\gamma\gamma$ and $ZZ^{(*)} \to 4l$ channels have been performed with the whole LHC dataset of 20.7 fb^{-1} at $\sqrt{s} = 8$ TeV and 4.8 fb^{-1} at $\sqrt{s} = 7$ TeV recorded by the ATLAS detector, allowing for refined property measurements. The signal observation is established in both individual channels with a significance above 6 σ. The new boson mass measurements reach a 0.5% accuracy in both channels, their compatibility and combination being discussed elsewhere [8]. Measurements of the signal strengths in different production processes are all consistent with a Standard Model Higgs boson, while spin-parity analyses do favour the SM expectation of 0^+ when compared pair-wise with 0^-, 1^+, 1^-, 2^+ and 2^-. These $H \to \gamma\gamma$ and $H \to ZZ^{(*)} \to 4l$ results are complemented with an analysis in the $H \to WW^{(*)} \to l\nu l\nu$ channel and a first search in the $H \to Z\gamma$ decay channel.

Updated measurements of the properties of the Higgs-like boson combining the diboson channels with fermionic decay studies [13] are reported elsewhere [8].

References

1. ATLAS collaboration, *Phys. Lett.* B **716** (2012) 1.
2. CMS collaboration, *Phys. Lett.* B **716** (2012) 30.
3. ATLAS collaboration, JINST **3** (2008) S08003.
4. ATLAS collaboration, ATLAS-CONF-2013-012, http://cds.cern.ch/record/1523698.
5. ATLAS collaboration, ATLAS-CONF-2012-168, http://cds.cern.ch/record/1499625.
6. ATLAS collaboration, ATLAS-CONF-2013-029, http://cds.cern.ch/record/1527124.
7. ATLAS collaboration, ATLAS-CONF-2013-013, http://cds.cern.ch/record/1523699.
8. B. Mansoulié, these proceedings.
9. LHC Higgs cross section working group, arXiv:1201.3084 [hep-ph]. CERN-2012-002.
10. ATLAS collaboration, ATLAS-CONF-2012-158, http://cds.cern.ch/record/1493601.
11. ATLAS collaboration, ATLAS-CONF-2013-030, http://cds.cern.ch/record/1527126.
12. ATLAS collaboration, ATLAS-CONF-2013-009, http://cds.cern.ch/record/1523683.
13. V. Martin, these proceedings.